Dalton Transactions

Accepted Manuscript

ROYAL SOCIETY OF CHEMISTRY

www.rsc.org/dalton

Understanding and Solving Disorder in Substitution Pattern of Amino Functionalized MIL-47(V)

Jurn Heinen, David Dubbeldam
Van 't Hoff Institute for Molecular Sciences, University of Amsterdam
Science Park 908, 1098 XH Amsterdam, The Netherlands

November 18, 2015

Abstract

Electronic energies and elastic constants of four amino functionalized MIL-47(V) supercells were computed using plane wave density functional theory to determine the influence of the substituent positions on the organic linker. An inverse relation between the ab initio energies and the elastic constants was found, indicating that high electronic stability correlates with high mechanical stability. A torsion in all supercells was induced upon substitution, which caused strain in the NH_2-MIL-47(V) supercell. The combined effect of the substituent bulkiness and the induced torsion reduced the pore volume of the NH_2-MIL-47(V) structures by $> 7\%$ and the surface area by $> 14\%$ with respect to MIL-47(V). This reduction was confirmed by a lower saturation capacity of methane, CO_2 and benzene. When unfavourable substituent positions are chosen, large torsions caused a further reduction of the saturation capacity. Differences in surface area, pore volume and saturation capacity illustrate the importance of chosing the correct NH_2-MIL-47(V) supercell.

Introduction

Metal-organic frameworks (MOFs), also known as coordination polymers, are a class of nanoporous materials consisting out of metal clusters interconnected with organic linkers. Due to their large surface area, high porosity and enormous number of synthesizable topologies, MOFs have promising applications in hydrogen,[1,2] CO_2[3] and methane[4] storage, adsorptive separation[5–7] and catalysis.[8,9] In contrast to other porous materials, such as zeolites, the pore characteristics of MOFs can be easily functionalized by substituting one or more hydrogens of the organic linker for various functional groups.[10–12] This can be achieved by prefunctionalizing the organic linkers or by post-synthetic modification. Functionalization of MOFs can, for example, heavily affect the breathing properties as was shown by Devic *et al.*[10] for the narrow pore - large pore transition of functionalized MIL-53(Fe).

An excellent example of a functionalized MOF was recently shown by Hu *et al.*[13] They constructed UTSA-100, an amino derivative of tetrazol-1,3-benzenedicarboxylic acid, that efficiently removes acetylene at room temperature from ethylene/acetylene mixtures containing only 1% of acetylene. Another interesting example is NH_2-MIL-88B(Fe) which improved the performance of multiple applications with respect to MIL-88B(Fe), such as acting as better photocatalyst for the reduction of Cr(VI)[14] and having a higher saturation capacity for ethanol, without given up the flexibility.[15] For NH_2-MIL-53(Fe) it was found to be an excellent solid base catalysts for the transesterication of triglycerides with methanol[16] and Serra-Crespo *et al.*[17] showed that it can be used in a vacuum pressure swing adsorption process for natural gas upgrading.

As described above, amino functionalized MOFs can provide improved performance for various applications. From single X-ray structures it is possible to determine the proper unit cell of the functionalized MOF; the question remains however, how these substituted linkers are distributed with respect to each other. This is important for modeling these materials, since it is expected that different substitution patterns,

resulting in linker-pair combinations, might lead to different adsorptive properties. For mono-substituted linkers there are numerous degrees of freedom with respect to the substituent positions, which is discussed below.

In this study, we address the substitution pattern of mono-amino functionalized MIL-47(V). MIL-47(V)[18] is a vanadium-based metalic cluster connected to BDC (= 1,4-benzenedicarboxylate) linkers and MIL-47(V) has the formula [V^{IV}(O)BDC]. In contrast to the MIL-53 family, MIL-47(V) is missing the μ_2-OH group due to thermal activation and does not show significant breathing.[19,20] The unit cell of MIL-47(V) is displayed in Figure 1a.

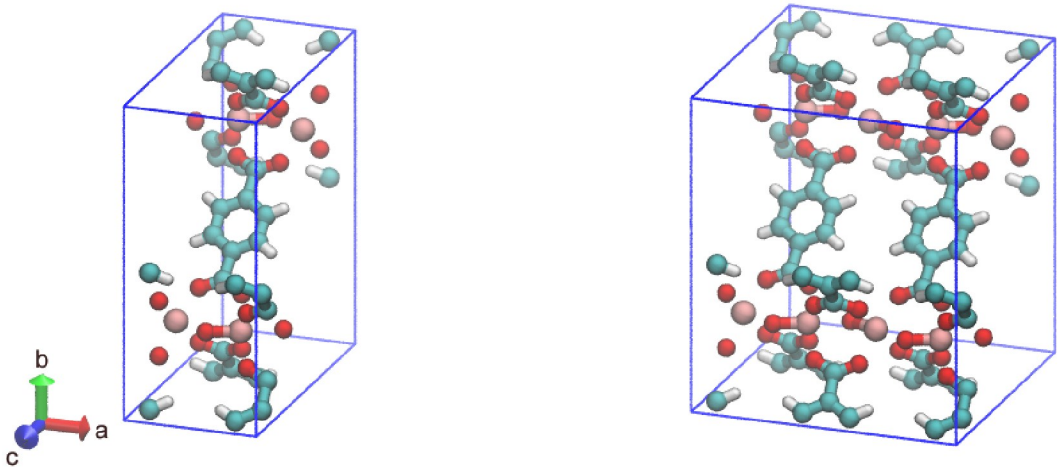

(a) (b)

Figure 1: Ball and stick model of (a) one, (b) two MIL-47(V) unit cells. The BDC-linkers of interest are displayed face-up. Cyan: C, red: O, pink: V, white: H.

Consider two MIL-47(V) unit cells along the a-axis that form a supercell; this results in adjacent BDC linkers, as shown in Figure 1b. Only the left/right ortho/meta positions of the aromatic ring of the BDC-linker are available for mono-substitution since the ipso and para positions are connected to the carboxylate. To our knowledge, it is currently unclear if the substituent positions on both BDC-linkers are identical or that they differ. We expect that the most stable structures are those with low energetics and high mechanical stability.

By comparing the *ab initio* energies and the elastic constants of the different linker-pair combinations, we can determine the effect that linker substitution has on the overall supercell. Furthermore, we computed single component adsorption isotherms (methane, CO_2 and benzene) and corresponding heat of adsorptions for the various isomeric supercells to illustrate the difference in adsorption properties (surface area and saturation capacity) due to these different linker-pair combinations.

Methodology

Approach

Two MIL-47(V) unit cells, see Figure 1b, each containing four BDC-linkers, were considered as a supercell to resemble two independent adjacent BDC-linkers. If only two adjacent BDC-linkers are substituted, this is called partial substitution which shows the local effect of two adjacent linkers upon substitution. Full substitution implies that all BDC-linkers are substituted and will reflect the overall effect on the supercell. The proposed substitution patterns are shown in Figure 2. A and B refer to the first and second BDC-linker, numbers indicate the positions of the aromatic ring with 1 = top ipso position and going clockwise until 6 = left ortho.

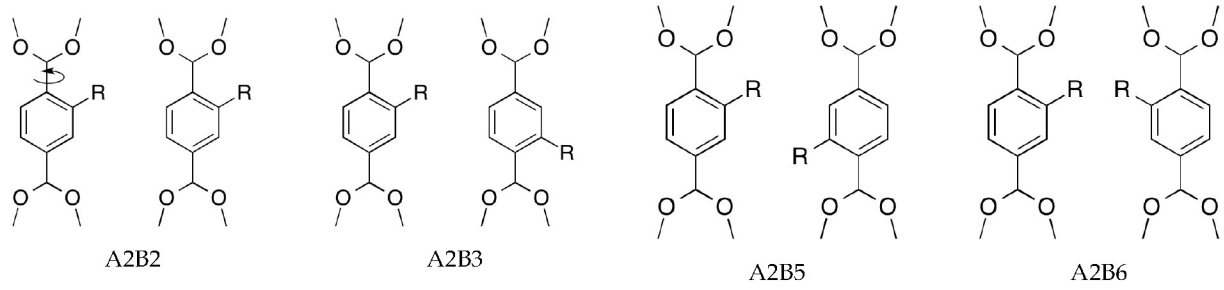

Figure 2: Four proposed linker-pair combinations of substituted BDC-linkers with substituent R = -NH_2. A/B refer to the left/right linker, whereas numbers indicate substituent positions. Only 2, 3, 5 and 6 are available for substitution. The dihedral angles ϕ_A and ϕ_B describe the torsion of both BDC-linkers as indicated by the arrow in the A2B2 configuration. When ϕ = 0°, the aromatic ring of BDC-linker is along the a-axis, for ϕ = 90° the aromatic ring is perpendicular to the a-axis.

Calculation of Relative Ab Initio Energies

To calculate the relative *ab initio* energies of the isomeric supercells, the geometry and lattice parameters of the structures were optimized using the Viena Ab Initio Software Package[21,22] (VASP) with the Grimme dispersion corrected[23] PBE[24] exchange-correlation functional. A plane wave basis was employed with an energy density cut-off of 600 eV in order to achieve high accuracy, needed for the computation of the stress tensor. Core-electrons were described by the projected augmented wave method[25,26] and integration in **k**-space was performed over the Γ-point using the Monkhorst-Pack sampling scheme.[27] A Gaussian electron smearing of 0.05 eV was applied to converge the electronic structure. Geometric convergence criteria of the ionic forces was set to 10^{-3} eV/Å.

Calculation of Elastic Constants

The mechanical and elastic properties of various MOFs have been studied intensively[28–30] and are essential to determine the stability of the supercells. A MOF subjected to a certain strain ϵ can be described by Hooks law (within the elastic limit) as[31]

$$\boldsymbol{\sigma}_i = \boldsymbol{\mathcal{C}}_{ij}\boldsymbol{\epsilon}_j \tag{1}$$

with $\boldsymbol{\sigma}_i$ being the stress tensor and $\boldsymbol{\mathcal{C}}_{ij}$ being the 6x6 elastic constant matrix in Voigt notation[1]. For a low symmetry orthorhombic unit cell, such as MIL-47(V), the elastic constant matrix has the form

[1] $\sigma_i = (\sigma_1 = \sigma_{xx}, \sigma_2 = \sigma_{yy}, \sigma_3 = \sigma_{zz}, \sigma_4 = \sigma_{yz}, \sigma_5 = \sigma_{xz}, \sigma_6 = \sigma_{xy})$

$$\boldsymbol{\mathcal{C}_{ij}} = \begin{pmatrix} C_{11} & C_{12} & C_{13} & & & \\ \cdot & C_{22} & C_{23} & & & \\ \cdot & \cdot & C_{33} & & & \\ & & & C_{44} & & \\ & & & & C_{55} & \\ & & & & & C_{66} \end{pmatrix} \tag{2}$$

with nine independent elastic constants. Dots indicate symmetry equivalent values. From the optimized structures, the elastic constants were computed using the same settings as described above. For the computation of the Hessian matrix, numerical derivatives were calculated using four displacements with the default value of 0.015 Å each.[32] VASP computes the elastic constants according to

$$\mathcal{C}_{ij} = \bar{\mathcal{C}_{ij}} - \frac{1}{V_0}\Lambda_{mi}\Big(\mathcal{H}^{-1}\Big)\Lambda_{nj}. \tag{3}$$

The first term of the r.h.s. of Eq. (3), known as the clamped ion term (or the Born term) is calculated by the stress-strain relation[33] for which six finite distortion (3 normal, 3 shear) of the lattice are applied, resulting in strained supercells. For each strain **E**, **E+e1**,..., **E+e6**, the corresponding stresses are computed *ab initio*. The clamped ionic elastic constants are than obtained by a least square fitting procedure as described by Paul and Saxe.[33]

The Born expression is generalized by including relaxation effects which are taken into account in the second term. The contributions due to relaxation of the elastic constants are calculated by multiplying the internal strain tensor Λ_{mj} with the inverted Hessian matrix $\mathcal{H}^{-1}$. Here, Λ_{mj} is the internal strain tensor[34] given by

$$\Lambda_{mj} = -V_0\Big(\frac{\partial^2 U}{\partial r_m \partial \epsilon_j}\Big) \tag{4}$$

with U is the energy per undeformed unit cell volume V_0 and r_m being the displacement of the atom from the equilibrium position. By subtracting the elastic moduli from ionic relaxation from the clamped ion term, we obtain the elastic constants.

It should be noted that by substituting the BDC-linkers, the symmetry of the supercell is destroyed and reducing the space group to P1. Therefore, the calculation of the elastic constants is subjected to numerical inaccuracies. For this reason, we also computed the elastic constants for MIL-47(V) in the P1 space group to assess trends in the elastic constants.

Calculation of Structural and Adsorption Properties

For the optimized structures we computed the pore volume, accessible surface area and single component adsorption isotherms using the molecular software package RASPA-2.0.[35] The void fraction is computed using the Widom particle insertion method[36] with helium as a probe at room temperature. Multiplying the helium void fraction by the total volume gives the pore volume.

The accessible surface area is calculated by the Shrake and Ruply method[37] in which a probe atom is used to 'roll' over the surface. It has been shown that the accessible surface area is a valid characteristic for describing the actual surface area of a MOF.[38] Values are close to surface areas obtained by the frequently used BET method.[38–40]

Single component adsorption isotherms for methane, CO_2 and benzene were computed using Grand Canonical Monte Carlo[41] simulations. Here, the temperature (T), chemical potential (μ) and volume (V) are fixed whereas the number of molecules are allowed to fluctuate.[42,43] We adapted the Configurational Bias Monte Carlo (CBMC) approach[44–46] where growth of the adsorbate molecules is biased towards favourable configurations. The amount of initialization cycles was set to 1000 and number of production cycles to 30000. Fugacity coefficients and excess loadings were computed using the Peng-Robinson equation[47] of state. For statistical purposes, the simulation is divided into five intervals. For each interval the standard

deviation within a 95% confidence interval was determined. The adsorbent interactions were described using the generic DREIDING[48] force field and adsorbates were described by the TraPPE force field.[49–51] Here, CO_2 is modelled as a tri-atomic molecule with partial atomic charges of 0.70e and -0.35e for C and O respectively to represent the quadrupole moment.[52] Framework charges[53] were computed using the REPEAT/ChelpG method[54,55] by fitting atomic charges on the *ab initio* electrostatic potential. The charge-charge interactions were computed using the Ewald summation[56] with a precision of 10^{-6} and the Van der Waals cut-off radius was set to 12.0 Å. Since MIL-47(V) does not show significant breathing upon adsorption, the framework atoms were kept rigid.

The heat of adsorption is computed using two methods: i) the Widom insertion method[36,43] and ii) the fluctuation theorema.[57,58] The heat of adsorption obtained from the the Widom insertion method[36,59] is computed according to

$$\Delta H = \langle U_{hg} \rangle - \langle U_g \rangle - \langle U_h \rangle - RT \tag{5}$$

with $\langle U_{hg} \rangle$ the host-guest (MOF-adsorbate) energy, $\langle U_g \rangle$ the energy of the guest and $\langle U_h \rangle$ the energy of the host. In the gas phase, we assume ideal behaviour and replace the PV-term by RT. Since the framework and guest are considered rigid, $\langle U_g \rangle$ = $\langle U_h \rangle$ = 0. The (isosteric) heat of adsorption within the energy-fluctuation theorema in the grand canonical ensemble[60] is often applied to non-zero loading and is computed according to[57,58]

$$\Delta H = \frac{\langle U \cdot N \rangle_\mu - \langle U \rangle_\mu \langle N \rangle_\mu}{\langle N^2 \rangle_\mu - \langle N \rangle_\mu \langle N \rangle_\mu} - \langle U_g \rangle - \beta^{-1}. \tag{6}$$

with $\langle \cdot\cdot \rangle$ being the average of either N, the amount of adsorbates or U, the internal energy, μ denotes the chemical potential and β the inverse temperature.

Results and Discussion

Lattice Parameters and Physical Properties

Table 1: Lattice parameters of NH_2-MIL-47(V) and MIL-47(V). Lattice vertices a, b and c in [Å], pore volume V_{pore} in [$Å^3$] and accessible surface area S_{ASA} in [m^2/g].

	a	b	c	α	β	γ	V_{pore}	S_{ASA}
MIL-47(V)	13.588	16.262	13.783	90.00	90.00	90.00	1823.40	1839.15
A2B2	13.578	16.386	13.653	90.05	90.17	90.37	1687.94	1589.82
A2B3	13.606	16.369	13.571	90.00	90.20	89.99	1685.58	1583.83
A2B5	13.584	16.569	13.433	90.06	90.27	90.27	1663.29	1560.84
A2B6	13.573	16.652	13.292	90.00	89.99	90.05	1536.21	1479.45

The optimized lattice parameters (Table 1) show that the amino functionalized MIL-47(V) supercells have angles that are not exactly 90°. The MIL-47 family members have orthorhombic space groups with angles of 90 degrees.[11,61] This implies that various orientations of the unit cells and various linker-pair combinations give on average, in the long range, cell parameters of α = β = γ = 90°.

The lattice axis a and lattice angle α are similar in the structures which can be attributed to the rigid metal-oxide bonds along the a-axis. Functionalizing MIL-47(V) reduces the pore volume and the effective surface area by > 150 $Å^3$ and > 200 m^2/g respectively. Two effects can be attributed to the pore volume and surface area reduction: the finite size of the substituent and the induced torsion due to the rotation of the BDC-linker described by the dihedral angles ϕ_A and ϕ_B (Table 2). Although A2B3 has the smallest torsions, the cell parameters deviate more than those of A2B6 which has significant larger dihedral angles (-14.20° and -10.88° vs. -2.21° and 2.52°).

Upon full substitution, configurations A2B2 and A2B5 show a decrease in the dihedral angles with respect to the partial substitution. This might imply that the full substitution reduces strain from the supercell for these configurations. Large dihedral angles of A2B6 are due to repulsive steric interactions caused by the amino groups and therefore result in significant lower pore volume and effective surface area. For A2B3, the sign of the dihedral angles differ, indicating that the BDC-linkers are twisted in opposite directions. Figure S1-A2B3 shows indeed that the geometry between V atoms is convex.

Table 2: Dihedral angles ϕ_A and ϕ_B of two adjacent BDC-linker in partial (two BDC-linkers substituted) and full (all BDC-linkers substituted) NH_2-MIL-47(V) supercells. Dihedral angle of MIL-47(V) is -1.05°.

	partial		full	
	ϕ_A	ϕ_B	ϕ_A	ϕ_B
A2B2	8.32	8.52	7.71	7.71
A2B3	-1.56	-5.05	-2.21	2.52
A2B5	7.45	9.76	6.14	6.35
A2B6	11.34	13.11	-14.20	-10.88

Relative Ab Initio Energies and Elastic Constants

Given the small energy difference ($\leq$ 2.00 kJ/mol) at 0 K, A2B2 and A2B5 are the most stable amino functionalized MIL-47(V) supercells for both partial and full substitution. At finite temperature, it is expected that from an energetic point of view, supercells A2B2 and A2B5 are equally likely. Despite the small dihedral angle of A2B3, the high relative *ab initio* energy indicates that this structure is energetic unfavourable. It is expected that this structure is strained due to the opposite positioning of the BDC-linkers. For A2B6 there is an unfavourable cooperative interaction upon substitution, since there is a factor 4.4 gain in *ab initio* energy going from partial to full substitution.

Table 3: Relative *ab initio* energies [kJ/mol] of partial and full NH_2-MIL-47(V).

	A2B2	A2B3	A2B5	A2B6
$\Delta E_{partial}$	0.00	12.94	0.55	13.68
ΔE_{full}	0.00	25.59	2.00	60.30

Figure 3 visualizes the nine independent elastic constants for the various NH_2-MIL-47(V) and MIL-47(V) supercells. Overall, the elastic constants for MIL-47(V) are higher than for any of the NH_2-MIL-47(V) supercells. Among the amino functionalized MIL-47(V) supercells, A2B2 and A2B5 have the highest elastic constants with the largest, absolute, difference for $\mathcal{C}_{22}$ with $\mathcal{C}_{22}$(A2B2) = 65.36 GPa and $\mathcal{C}_{22}$(A2B5) = 75.60 GPa. The clamped ionic term $\bar{\mathcal{C}_{22}}$ for A2B2 is 117.74 Gpa and 123.54 GPa for A2B5 and the contributions due to relaxation for A2B2 and A2B5 are -52.38 Gpa and -47.94 Gpa respectively.

The amino groups of the adjacent linkers are in proximity of each other for A2B5, see Figure 2 and Figure S3. Note that the linkers have a torsion and thus the nitrogens have different positions along the b-axis. Straining along the b-axis reduces the nitrogen-nitrogen distance resulting in a repelling interaction which gives a more rigid structure. This repelling nitrogen-nitrogen behaviour is not present in A2B2.

An inverse trend between the relative *ab initio* energies and the elastic constants can be observed. NH_2-MIL-47(V) supercells that have high *ab initio* energies (A2B3 and A2B6) have lower elastic constants, whereas supercells that have low *ab initio* energies (A2B2 and A2B5) have high elastic constants. It is not clear if this relation holds for other functionalized MIL-47(V) structures.

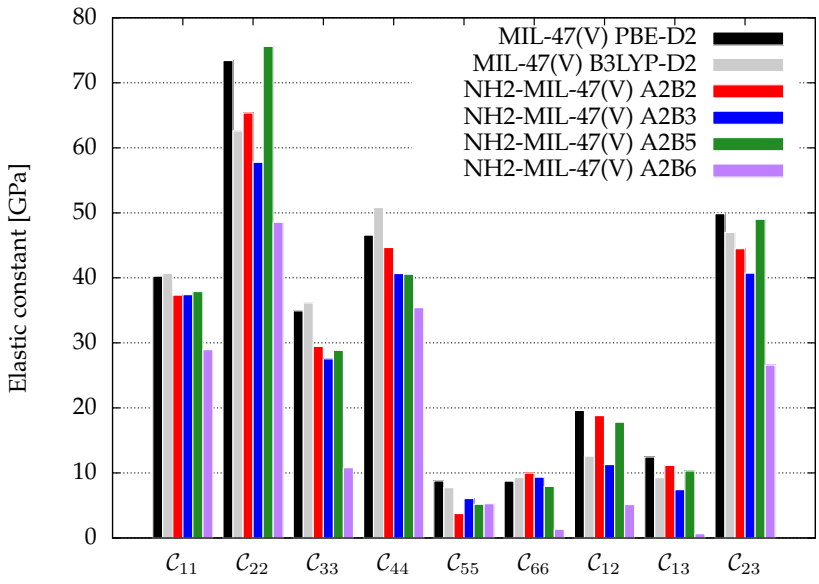

Figure 3: The nine independent elastic constants C_{ij} in Voigt notation of MIL-47(V) and the four isomeric NH_2-MIL-47(V) supercells. MIL-47(V) has been computed by Ortiz. *et al.*[62,63] at the B3LYP-D2 level.

Single Component Adsorption Isotherm

The amino functionalized MIL-47(V) structures have lower surface area's than MIL-47(V) (Table 1) and this can also be observed from the saturation capacity for methane and CO_2 as shown in Figure 4 and for benzene in Figure S2. In particular for A2B6 this effect is more profound.

At lower pressures the CO_2 isotherms differ, whereas for methane the isotherms are identical. For CO_2 this difference is expected due to the dominating sorbent-adsorbate interaction given between the quadrupole moment of CO_2 and the amino group. Comparing heat of adsorptions at infinite dilution in Table 4 shows that the simulated trend agrees with the experimental trend: larger heat of adsorption for the amino functionalized MIL-47(V). Similar behaviour has been observed between MIL-53(Al) and NH_2-MIL-53(Al).[64] At finite loading, it is also observed, see Figure S4, that the heat of adsorption is more favourable for NH_2-MIL-47(V) than for MIL-47(V) for methane and CO_2 adsorption. At higher loadings, the heat of adsorptions changes due to adsorbate-adsorbate interactions (Figure S5). The heat of adsorption for CO_2 is larger than for methane as expected, although there is a slight difference between experimental and computational results. This difference is attributed to the rigidity of the force field framework; upon CO_2 adsorption, the amino group is no longer in the same plane as the BDC-linker. Optimized VASP structures from Leus *et al.*[61] show a dihedral angle of -15.20° with the hydrogens pointing away. The heat of adsorption difference among the various supercells is negligible and not suprising since CO_2 will adsorb most-likely on the nitrogen of the amino group which is irrevant of the substitution pattern of the linkers. The combined effect of the substituted linker can alter the adsorption positions at higher loadings.

At saturation loadings the isotherms changes for both adsorbates. Leus *et al.*[61] measured experimentally the single component isotherms for methane and CO_2 at T = 303 K for MIL-47(V) and NH_2-MIL-47(V) with a saturation capacity for CO_2 and CH_4 in MIL-47(V) of 7.7 and 4.1 mol/kg respectively. The simulated saturation capacities are higher than the experimental ones, which is a general feature since for simulated isotherms, defects and impurities are not taken into account.

For larger adsorbates, the influence of the substitution patterns are more significant. Figure S2 shows the computed single component adsorption isotherms for benzene at 328 K. Steeper uptakes of the benzene adsorption isotherms for NH_2-MIL-47(V) are observed and indicate that benzene adsorbs stronger in

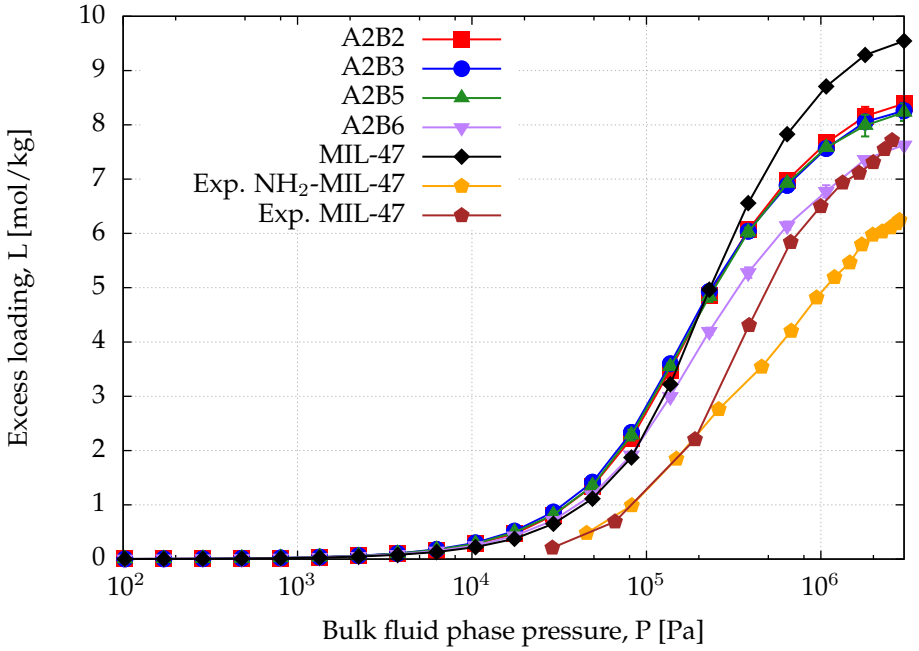

(a)

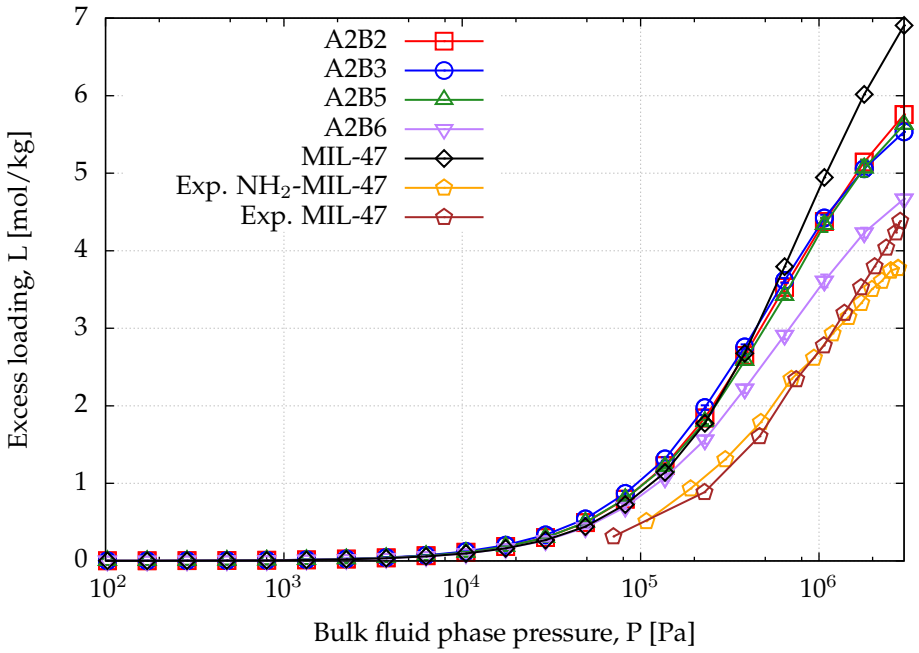

(b)

Figure 4: CB-GCMC adsorption isotherms of (a) CO_2 (b) methane for MIL-47(V) and NH_2-MIL-47(V) at T = 303 K. Standard deviations of methane and CO_2 isotherms are smaller than symbol sizes. Experimental saturation capacities for CO_2 and methane uptake in NH_2-MIL-47(V) are and 6.2 and 3.6 mol/kg.[61]

NH_2-MIL-47(V) than in MIL-47(V). This is not a confinement effect, which has been observed for benzene adsorption in zeolite MFI,[65] since benzene is approximately 5.5 Å in size and the pore diameter of MIL-47(V) is 10.5 and 11.0 Å.[66] However, at high pressures, the saturation capacity of MIL-47(V) for benzene is higher than for NH_2-MIL-47(V) due to better packing of the benzene adsorbates.

Table 4: Experimental and CBMC heat of adsorption in [kJ/mol] for CO_2 and methane computed at 303 K using Widom particle insertion method.

	ΔH_{ads}	
	CO_2	methane
MIL-47(V)	-19.06	-15.55
A2B2 NH_2-MIL-47(V)	-20.73	-16.57
A2B3 NH_2-MIL-47(V)	-20.90	-16.82
A2B5 NH_2-MIL-47(V)	-20.89	-16.57
A2B6 NH_2-MIL-47(V)	-20.71	-16.48
Exp.[61] MIL-47(V)	-17.8	-11.1
Exp.[61] NH_2-MIL-47(V)	-22.0	-13.0

Conclusions

We demonstrated that various linker-pair combinations of amino functionalized MIL-47(V) affect structural and adsorption properties of the sorbent. Functionalizing MIL-47(V) with amino groups reduces the accessible surface area, pore volume and the saturation capacities for methane, CO_2 and benzene. Heat of adsorption at infinite dilution for various linker-pair combinations are equal, indicating that different substitution patterns do not affect adsorption in the Henry regime. As a result of linker substitution, torsions of the BDC-linker induce strain in the material leading to both energetic and mechanical unstable structures. An inverse relation between the relative *ab initio* energy and elastic constants was observed. It is therefore crucial to consider the appropiate unit cell in simulation studies. For amino functionalized MIL-47(V), A2B2 and A2B5 are the most stable structures.

Associated Content

Supporting Information
Figures of the four amino functionalized MIL-47(V), viewed along the a-axis. Benzene adsorption isotherms at T = 328 K. Heat of adsorption as finite loading.

Author Information

Corresponding Author
E-mail: J.Heinen@uva.nl
Notes
The authors declare no competing financial interest.

Acknowledgements

This material is supported by the Netherlands Research Council for Chemical Sciences (NWO/CW) through a VIDI grant (David Dubbeldam). We thank Sofia Calero and Ariana Torres-Knoop for fruitful discussions

and SURFsara (www.surfsara.nl) for the support in using the Lisa Compute Cluster.

References

[1] Murray, L. J.; Dinca, M.; Long, J. R. *Chem. Soc. Rev.* **2009**, *38*, 1294–1314.
[2] Han, S. S.; Mendoza-Cortes, J. L.; Goddard III, W. A. *Chem. Soc. Rev.* **2009**, *38*, 1460–1476.
[3] Zhang, Z.; Yao, Z.-Z.; Xiang, S.; Chen, B. *Energy Environ. Sci.* **2014**, *7*, 2868–2899.
[4] He, Y.; Zhou, W.; Qian, G.; Chen, B. *Chem. Soc. Rev.* **2014**, *43*, 5657–5678.
[5] Van de Voorde, B.; Bueken, B.; Denayer, J.; De Vos, D. *Chem. Soc. Rev.* **2014**, *43*, 5766–5788.
[6] Li, J.-R.; Sculley, J.; Zhou, H.-C. *Chem. Rev.* **2012**, *112*, 869–932.
[7] Torres-Knoop, A.; Dubbeldam, D. *Chem.Phys.Chem* **2015**, 2046–2067.
[8] Chughtai, A. H.; Ahmad, N.; Younus, H. A.; Laypkov, A.; Verpoort, F. *Chem. Soc. Rev.* **2015**,
[9] Liu, J.; Chen, L.; Cui, H.; Zhang, J.; Zhang, L.; Su, C.-Y. *Chem. Soc. Rev.* **2014**, *43*, 6011–6061.
[10] Devic, T. et al. *J. Am. Chem. Soc.* **2010**, *132*, 1127–1136.
[11] Biswas, S.; Vanpoucke, D. E. P.; Verstraelen, T.; Vandichel, M.; Couck, S.; Leus, K.; Liu, Y.-Y.; Waroquier, M.; Speybroeck, V. V.; Denayer, J. F. M.; Voort, P. V. D. *J. Phys. Chem. C* **2013**, *117*, 22784–22796.
[12] Lu, W.; Wei, Z.; Gu, Z.-Y.; Liu, T.-F.; Park, J.; Park, J.; Tian, J.; Zhang, M.; Zhang, Q.; Gentle III, T.; Bosch, M.; Zhou, H.-C. *Chem. Soc. Rev.* **2014**, *43*, 5561–5593.
[13] Hu, T.-L.; Wang, H.; Li, B.; Krishna, R.; Wu, H.; Zhou, W.; Zhao, Y.; Han, Y.; Wang, X.; Zhu, W.; Yao, Z.; Xiang, S.; Chen, B. *Nat. Commun.* **2015**, *6*, 7328.
[14] Shi, L.; Wang, T.; Zhang, H.; Chang, K.; Meng, X.; Liu, H.; Ye, J. *Adv. Sci.* **2015**, *2*, doi: 10.1002/cphc.201500195.
[15] Scherb, C.; Williams, J. J.; Hinterholzinger, F.; Bauer, S.; Stock, N.; Bein, T. *J. Mater. Chem.* **2011**, *21*, 14849–14856.
[16] Chen, J.; Liu, R.; Gao, H.; Chen, L.; Ye, D. *J. Mater. Chem. A* **2014**, *2*, 7205–7213.
[17] Serra-Crespo, P.; Wezendonk, T. A.; Bach-Samario, C.; Sundar, N.; Verouden, K.; Zweemer, M.; Gascon, J.; Berg, H. v. d.; Kapteijn, F. *Chem. Eng. Technol.* **2015**, *38*, 1183–1194.
[18] Barthelet, K.; Marrot, J.; Riou, D.; Ferey, G. *Ang. Chem. Int. Ed.* **2002**, *41*, 281–284.
[19] Salles, F.; Jobic, H.; Devic, T.; Llewellyn, P. L.; Serre, C.; Férey, G.; Maurin, G. *ACS Nano* **2010**, *4*, 143–152.
[20] Rosenbach, N.; Jobic, H.; Ghoufi, A.; Salles, F.; Maurin, G.; Bourrelly, S.; Llewellyn, P.; Devic, T.; Serre, C.; Férey, G. *Angew. Chem. Int. Ed.* **2008**, *47*, 6611–6615.
[21] Kresse, G.; Hafner, J. *Phys. Rev. B* **1994**, *49*, 14251–14269.
[22] Kresse, G.; Furthmüller, J. *Phys. Rev. B* **1996**, *54*, 11169–11186.
[23] Grimme, S.; Antony, J.; Ehrlich, S.; Krieg, H. *J. Chem. Phys.* **2010**, *132*, 154104.
[24] Perdew, J. P.; Burke, K.; Ernzerhof, M. *Phys. Rev. Lett.* **1996**, *77*, 3865–3868.
[25] Blöchl, P. *Phys. Rev. B* **1994**, *50*, 17953–17979.
[26] Kresse, G.; Joubert, D. *Phys. Rev. B* **1999**, *59*, 1758–1775.
[27] Monkhorst, H. J.; Pack, J. D. *Phys. Rev. B* **1976**, *13*, 518892.
[28] Tan, J. C.; Cheetham, A. K. *Chem. Soc. Rev.* **2011**, *40*, 1059–1080.
[29] Tan, J.-C.; Civalleri, B.; Lin, C.-C.; Valenzano, L.; Galvelis, R.; Chen, P.-F.; Bennett, T. D.; Mellot-Draznieks, C.; Zicovich-Wilson, C. M.; Cheetham, A. K. *Phys. Rev. Lett.* **2012**, *108*, 095502.
[30] Li, W.; Henke, S.; Cheetham, A. K. *APL Materials* **2014**, *2*, 1–9.
[31] Nye, J. F. *Physical Properties of Crystals: Their Representation by Tensors and Matrices*; Oxford Science Publications, 1984.
[32] VASP Manual. http://cms.mpi.univie.ac.at/VASP.
[33] Le Page, Y.; Saxe, P. *Phys. Rev. B* **2002**, *65*, 104104.
[34] Wu, X.; Vanderbilt, D.; Hamann, D. R. *Phys. Rev. B* **2005**, *72*, 035105.
[35] Dubbeldam, D.; Calero, S.; Ellis, D.; Snurr, R. RASPA 2.0: Molecular Software Package for Adsorption and Diusion in (Flexible) Nanoporous Materials. 2015; `http://dx.doi.org/10.1080/08927022.2015.1010082`.
[36] Widom, B. *J. Chem. Phys.* **1963**, *39*, 2808–2812.

[37] Shrake, A.; Rupley, J. *J. Mol. Bio.* **1973**, *79*, 351 – 371.
[38] Düren, T.; Millange, F.; Férey, G.; Walton, K. S.; Snurr, R. Q. *J. Phys. Chem. C* **2007**, *111*, 15350–15356.
[39] Brunauer, S.; Emmett, P. H.; Teller, E. *J. Am. Chem. Soc.* **1938**, *60*, 309–319.
[40] Walton, K. S.; ; Snurr, R. Q. *J. Am. Chem. Soc.* **2007**, *129*, 8552–8556.
[41] Nicholson, D.; Parsonage, N. G. *Computer simulation and the statistical mechanics of adsorption*; New York: Academic Press, 1988.
[42] Dubbeldam, D.; Torres-Knoop, A.; Walton, K. S. *Mol. Sim.* **2013**, *39*, 1253–1292.
[43] Frenkel, D.; Smit, B. *Understanding Molecular Simulation: From Algorithms to Applications*, 2nd ed.; Academic Press, 2002.
[44] Siepmann, J. I. *Mol. Phys.* **1990**, *70*, 1145–1158.
[45] Siepmann, J. I.; Frenkel, D. *Mol. Phys.* **1992**, *75*, 59–70.
[46] Frenkel, D.; Mooij, G. C. A. M.; Smit, B. *J. Phys.: Condens. Matter* **1992**, *4*, 3053.
[47] Peng, D.-Y.; Robinson, D. B. *In. Eng. Chem. Fundam.* **1976**, *15*, 59–64.
[48] Mayo, S. L.; Olafson, B. D.; Goddard, W. A. *J. Phys Chem.* **1990**, *94*, 8897–8909.
[49] Potoff, J. J.; Siepmann, J. I. *AIChE J.* **2001**, *47*, 1676–1682.
[50] Martin, M. G.; Siepmann, J. I. *J. Phys. Chem. B* **1998**, *102*, 2569–2577.
[51] Rai, N.; Siepmann, J. I. *J. Phys. Chem. B* **2007**, *111*, 10790–10799.
[52] Harris, J. G.; Yung, K. H. *The Journal of Physical Chemistry* **1995**, *99*, 12021–12024.
[53] Hamad, S.; Balestra, S. R.; Bueno-Perez, R.; Calero, S.; Ruiz-Salvador, A. R. *J. Solid State Chem.* **2015**, *223*, 144151.
[54] Campañá, C.; Mussard, B.; Woo, T. K. *J. Chem. Theory Comput.* **2009**, *5*, 2866–2878.
[55] Watanabe, T.; Manz, T. A.; Sholl, D. S. *J. Phys. Chem. C* **2011**, *115*, 4824–4836.
[56] Ewald, P. P. *Ann. Phys.* **1921**, *369*, 253–287.
[57] Nicholson, D.; Parsonage, N. G. *Computer simulation and the statistical mechanics of adsorption*; New York, USA, Academic Press, 1982.
[58] Vlugt, T. J. H.; Garcia-Perez, E.; Dubbeldam, D.; Ban, S.; ; Calero, S. *J. Chem. Theory Comput.* **2008**, *4*, 11071118.
[59] Vlugt, T. J. H. *Mol. Simul.* **1999**, *23*, 63.
[60] Karavias, F.; Myers, A. L. *Langmuir* **1991**, *7*, 3118.
[61] Leus, K.; Couck, S.; Vandichel, M.; Vanhaelewyn, G.; Liu, Y.-Y.; Marin, G. B.; Driessche, I. V.; Depla, D.; Waroquier, M.; Speybroeck, V. V.; Denayer, J. F. M.; Voort, P. V. D. *Phys. Chem. Chem. Phys.* **2012**, *14*, 15562–15570.
[62] Ortiz, A. U.; Boutin, A.; Fuchs, A. H.; Coudert, F.-X. *Phys. Rev. Lett.* **2012**, *109*, 195502.
[63] Ortiz, A. U.; Boutin, A.; Fuchs, A. H.; Coudert, F.-X. *J. Chem. Phys.* **2013**, *138*, 174703.
[64] Torrisi, A.; Bell, R. G.; Mellot-Draznieks, C. *Microporous and Mesoporous Materials* **2013**, *168*, 225 – 238.
[65] Clark, L. A.; Snurr, R. Q. *Chem. Phys. Lett.* **1999**, *308*, 155 – 159.
[66] Tanaka, D.; Nakagawa, K.; Higuchi, M.; Horike, S.; Kubota, Y.; Kobayashi, T.; Takata, M.; Kitagawa, S. *Angew. Chem. Int. Ed.* **2008**, *47*, 3914–3918.